Laser Melting of Ti-15Al-20Nb Alloy

B.S. Yilbas and M. Sami

Titanium aluminides have become promising materials for high-temperature applications, but the relatively poor oxidation resistance and elevated-temperature strength of these alloys limit their application to temperatures lower than 1000 °C. Niobium addition improves the properties of titanium aluminide. However, the mechanical, metallurgical, and corrosion properties of Ti-Al-Nb may be improved by treatment with a laser beam. Consequently, the present study examines the properties of Ti-15Al-20Nb alloy subjected to the Nd:YAG laser melting process. Hardness in the surface region increases to twice the base material hardness, and corrosion resistance improves considerably after laser treatment.

Keywords
laser melting, surface treatment, thermal transfer, titanium alloys

1. Introduction

MODERN industry continues to demand lightweight materials that can withstand service temperatures greater than 950 K. Extended service at such elevated temperatures, however, requires materials with extremely stable microstructures. It has been well established that intermetallic compounds remain stable and maintain very high strength levels at high temperatures, but are extremely brittle at room temperature (Ref 1). One of the promising intermetallics is titanium aluminide, which possesses good combinations of high strength, low density, and superior oxidation resistance at elevated temperatures. The titanium aluminides (TiAl and Ti_3Al) are inherently brittle owing to their ordered crystal structures, which reduce the number of available slip systems (Ref 2). Due to the room-temperature slip behavior of intermetallic alloys, crack nucleation and propagation becomes the preferred deformation mode.

Many solutions addressing the problem of poor ductility of intermetallic alloys have been introduced (Ref 3, 4). Major attempts to improve low ductility focus on altering the crystal structure through alloying without sacrificing material strength. It has been shown that reducing the slip distance, by creating a small grain-size structure, reduces planar slip behavior of ordered intermetallics (Ref 4). Niobium has proved to be the most effective addition for improving the properties of titanium aluminides.

The phase constitution map, density variation, oxidation and corrosion resistance map, and mechanical properties of the ternary Ti-Al-Nb system were systematically studied (Ref 5). It was shown that this system is a potential replacement for conventional titanium and nickel-base alloys. However, welding of such alloy parts is extremely difficult because the moderate cooling rates associated with conventional arc welding processes promote the formation of a fine Widmanstätten α_2 structure that exhibits high hardness and low ductility (Ref 3). Consequently, study into rapid solidification using laser-beam technology becomes essential to investigate the mechanical and metallurgical properties of the resulting melts.

In light of these findings, the present study investigated the mechanical and metallurgical properties of Ti-15Al-20Nb alloy melted by a neodymium:yttrium-aluminum-garnet (Nd:YAG) laser. A pulsed Nd:YAG laser was used to generate a rapidly cooled fusion-zone microstructure in Ti-15Al-20Nb composed of a potentially ductile ordered β phase. In order to validate the theoretical model, the study was extended to include experimental measurement of the surface temperature of the laser-irradiated spot. This was achieved using an optical method. Microhardness tests were carried out across the melt cross sections. The corrosion resistance of both laser-treated and untreated alloy was also investigated.

B.S. Yilbas and **M. Sami,** Department of Mechanical Engineering, King Fahd University of Petroleum and Minerals, Dhahran, Saudi Arabia.

2. Mathematical Modeling

2.1 *Heat-Transfer Model*

A new model for examining the laser heating process has been developed using the electron-kinetic theory (Ref 6). This approach describes the transport of energy through electron-phonon collisions. Some useful assumptions are made for simplicity. Steady-state space charge is assumed, in which exactly the same number of electrons is emitted from the material as is returning from the space charge; this allows energy losses due to thermionic emission to be neglected. Energy-transfer processes occur due to electron-phonon collisions; immediately after the collision, the electrons may change their directions, but the electron flux remains constant in any direction. During the collision, some fraction of the excess electron energy is transferred to the phonons. In the solution, local equilibrium is assumed to prevail at $t = 0$ when material is at a uniform temperature.

In this analysis, the electron-phonon collision was assumed to occur such that before and after the collision, the colliding electron had the same kinetic energy and thus the same momentum. In other words, collisions were assumed to be elastic (Ref 6).

At temperature T, the average energy associated with the lattice is given by Planck's formula (Ref 7):

$$E = \frac{hw_g}{(e^{(hw_g)/(k_B T)} - 1)}$$

The total energy-transfer equation can be written as (Ref 6):

$$N A(E_{x,t+dt} - E_{x,t})\,dx = I_0\delta \exp(-\delta x) A\,dt\,dx + \int_{-\infty}^{\infty} \frac{N v}{6\lambda^2} \exp\left\{-\frac{|x-s|}{\lambda}\right\} f(E_{s,t} - E_{x,t})\,ds\,A\,dt\,dx \quad \text{(Eq 1)}$$

After arranging the total energy-transfer equation, the lattice temperature gradients can be written as:

$$\frac{dT(x,t)}{dt} = \frac{I_0\delta}{\rho C_p}\exp(-\delta x) - \frac{Kf}{2\lambda^2 \rho C_p} T(x,t) + \frac{Kf}{4\lambda^3 \rho C_p}\left[\int_0^{\infty} \exp\left(-\frac{|x+s|}{\lambda}\right) T(s,t)\,ds + \int_0^{x} \exp\left(-\frac{|x-s|}{\lambda}\right) T(s,t)\,ds + \int_x^{\infty} \exp\left(-\frac{|x-s|}{\lambda}\right) T(s,t)\,ds\right] \quad \text{(Eq 2)}$$

Details of the above derivation can be found in Ref 6.

The rate at which the melting front is moving is determined by the rate of heat transfer per unit volume used in melting process. This heat-transfer rate is given by:

$$\rho C_p V_m \frac{\partial T}{\partial x}$$

The velocity of the melting surface:

$$V_m = \frac{I_0}{\rho[C_p T_s + L(T_s)]}$$

where

$$L(T_s) = L_0\left[1 - \left(\frac{T}{T_c}\right)^2\right]^{1/2}$$

are simultaneous equations in V_m and T_s. They constitute conditions under which the surface will recede at a constant rate. This is true even for temperatures below the standard boiling temperature provided that the evaporation takes place in vacuum.

Incorporating this convection term in the energy equation yields:

$$\frac{dT(x,t)}{dt} = \frac{I_0\delta}{\rho C_p}\exp(-\delta x) - f\frac{K}{2\lambda^2} T(x,t) + \frac{Kf}{4\lambda^3}\left[\int_0^{\infty} \exp\left(-\frac{|x+s|}{\lambda}\right) T(s,t)\,ds + \int_0^{x} \exp\left(-\frac{|x-s|}{\lambda}\right) T(s,t)\,ds + \int_x^{\infty} \exp\left(-\frac{|x-s|}{\lambda}\right) T(s,t)\,ds\right] + V_m\left(\frac{\partial T}{\partial x}\right) \quad \text{(Eq 3)}$$

Equation 3 is in the form of an integro-differential equation and does not yield to analytic solution due to the mathematical complexities involved. Hence, a numerical method is employed. A computer program has been developed that solves the energy equation using an explicit finite-difference scheme. The results are presented for the Ti-Al-Nb alloy system.

3. Experimental Method

The experimental setup is shown in Fig. 1. An Nd:YAG laser delivering 20 J within 1.48 ms pulses was used to irradiate the workpiece. The pulse rate of the laser was set to 50 Hz, which was the maximum attainable repetition rate. A 51 mm focal-length lens was used to focus the laser beam. To obtain shielding from oxygen, a vacuum chamber was designed using helium as a shielding gas. The alloy samples were received in the form of $\alpha_2 + \beta$ processed sheet of 2 mm thickness. To validate the numerical predictions, an experiment was carried out to measure the surface temperature of the laser-irradiated spot.

The principle of the temperature measurement is that for a given temperature, a unique ratio of monochromatic emissive power intensities corresponds to two spectral frequencies. By measuring this emissive power ratio, the corresponding surface temperature can be calculated. The temporal surface temperature can be determined knowing the time-dependent emissive power ratios correspond to two spectral frequencies.

Spectral analysis of the light emitted from the heated spot was performed using a grating spectrometer (Fig. 1). The spectral intensity at two wavelengths was recorded using RCA 30818 fast-response photodiodes with integrated amplifiers spaced 2 cm apart at the exit slit of the spectrometer, which was positioned 45° to the incident laser beam. Light emitted from the heated spot was focused onto the inlet slit of the spectrome-

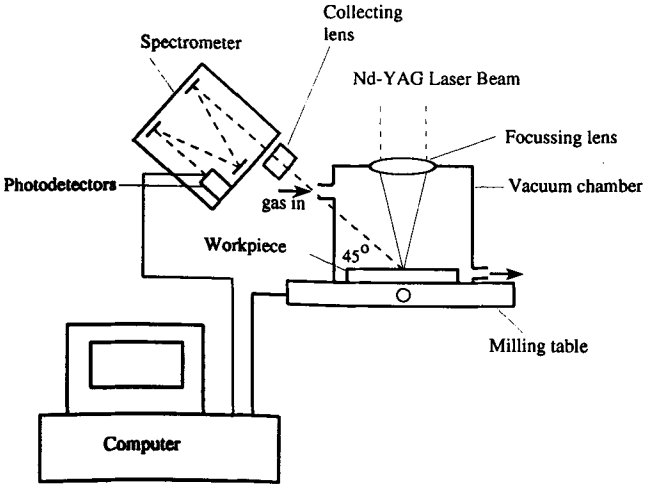

Fig. 1 Experimental setup

ter. This was achieved through use of two f6.3 glass lenses transmitting in the 0.28 to 1.7 μm range with a focal length of 500 mm. Details of the measurement are not given here but are referred to in Ref 8.

After completion of the laser melting process, samples were sectioned, mounted, polished, and etched with Kroll's reagent ($HF + HNO_3$). Scanning electron microscopy and optical microscopy were carried out to examine the metallurgical changes in the melt cross sections, which were also microhardness tested. The corrosion properties of laser-treated and untreated samples were tested using an anodic corrosion test. A $2N$ H_2SO_4 solution was used at room temperature. The corrosion experiment was carried out using an EG&G 273 A instrument.

4. Results and Discussion

Figure 2 shows temporal variation of the surface temperature rise predicted theoretically and obtained experimentally for the laser heating pulse. The surface temperature rises rapidly to the melting temperature and, once melting starts, remains almost constant. This is because the absorbed laser energy is dissipated through melting, conduction, and internal energy gain by the workpiece. The energy balance among these processes occurs such that the internal energy of the workpiece at the surface remains constant, which in turn results in a constant surface temperature. It should be noted that the convection and radiation losses from the surface during the laser heating pulse is omitted in the analysis. Comparison of the theoretical predictions with the experimental results shows that both are in good agreement. However, the discrepancies occurring at elevated temperatures between results may be due to the assumptions made in the theory and/or experimental error, which is estimated as 7%. At elevated temperatures, the emissive power ratios calculated fall to unity (Ref 8); therefore, the corresponding temperatures become difficult to measure with sufficient accuracy.

Table 1 Polarization resistance results

Condition	Polarization resistance, kΩ/cm²	I_{corr}, μA/cm²	Corrosion rate, mm/yr
Untreated	6.75	3.25	0.038
Laser treated	7.25	2.82	0.032

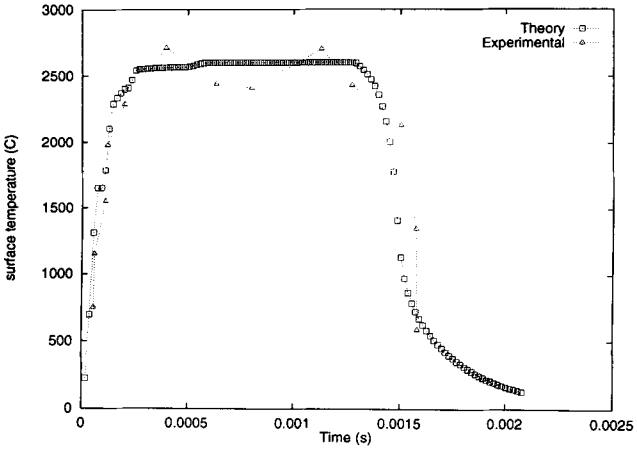

Fig. 2 Temporal variation of surface temperatures predicted theoretically and obtained experimentally

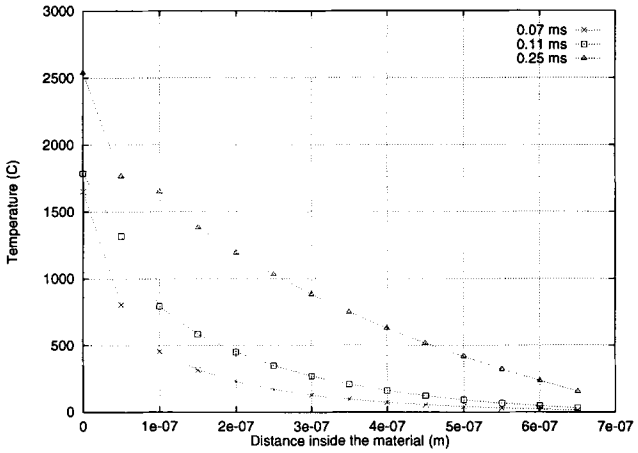

Fig. 3 Temperature profiles inside the workpiece at different times

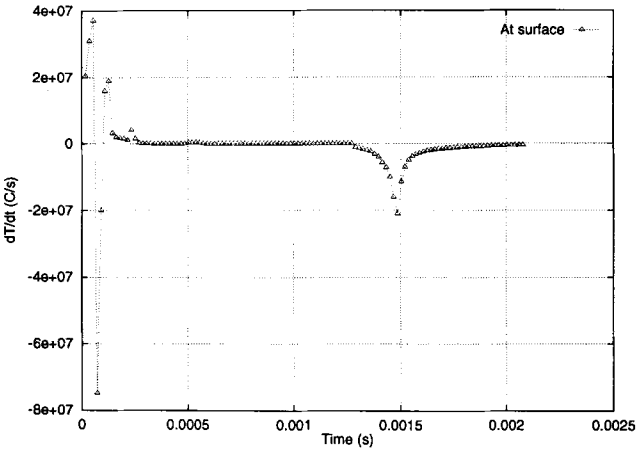

Fig. 4 Variation of dT/dt with time

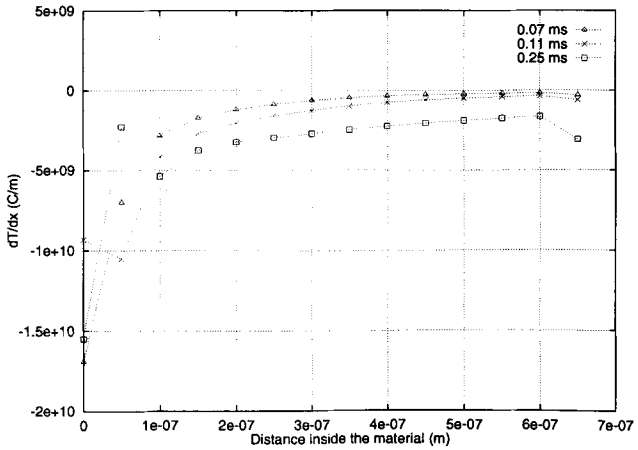

Fig. 5 Variation of dT/dx

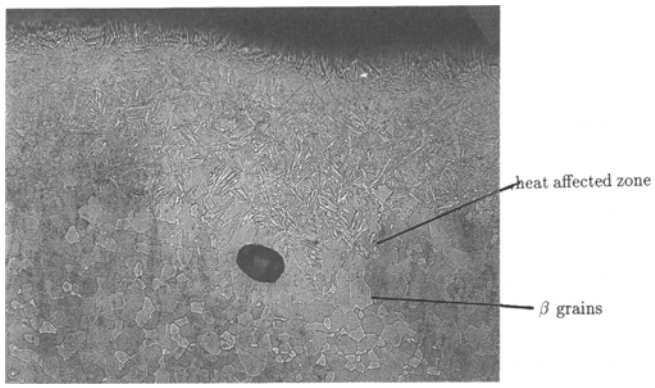

(a)

(b)

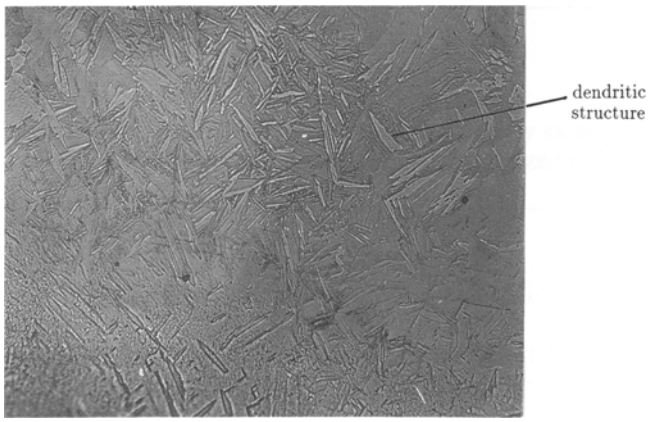

(c)

Fig. 6 Optical micrographs of workpiece. (a) 100×. (b) 200×. (c) 300×

Figure 3 shows the temperature profiles inside the workpiece predicted at different heating times. As the heating time increases, the temperature inside the workpiece increases rapidly, resulting in high surface temperature (i.e., $\partial T/\partial x = 10^8$ K/m). This may be because the energy gain by the workpiece is higher than that dissipated through conduction.

Figure 4 shows the variation of dT/dt with heating time. It is evident that a heating rate on the order of 0.2×10^6 K/s occurs

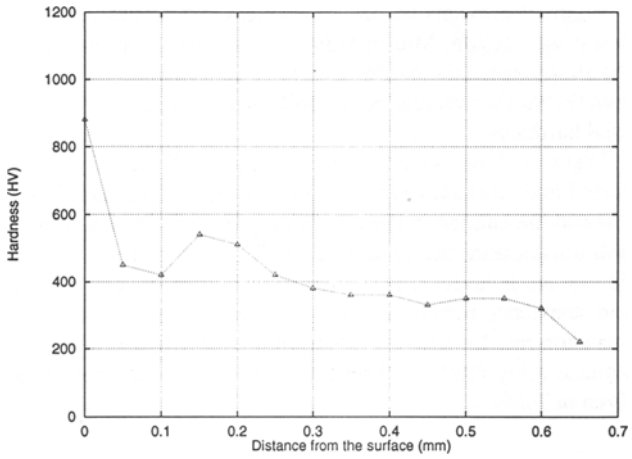

Fig. 7 Microhardness test results

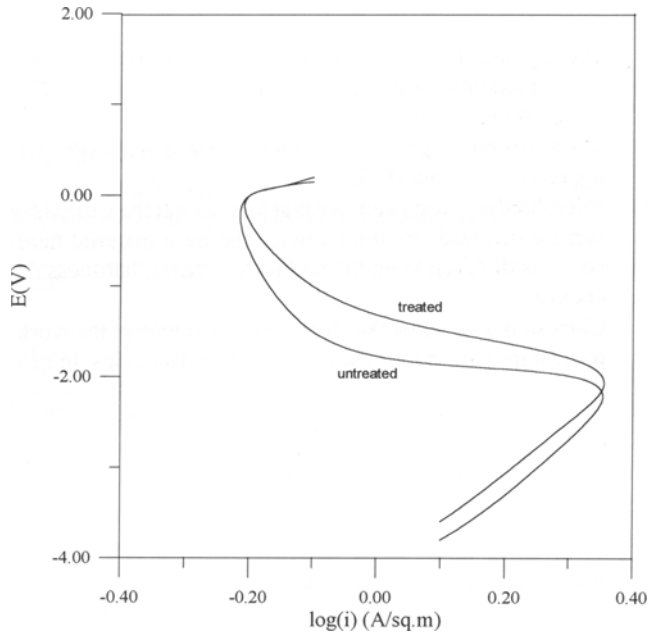

Fig. 8 Anodic polarization test results

at the beginning of the pulse. However, as the heating pulse progresses, the cooling cycle initiates and the cooling rate is on the order of 10^5 K/s. Figure 5 shows the temperature gradient with distance below the surface. The temperature gradient in the surface region is extremely high during the initial heating pulse, but reduces as heating progresses.

The optical micrographs in Fig. 6 reveal that a narrow heat-affected zone (HAZ) occurs directly adjacent to the fusion boundary. Study of the fusion-boundary region detected columnar β grains growing epitaxially from the base metal substrate in toward the center of the fusion zone. Evidence of a cellular dendritic solidification substructure confirmed the partitioning of niobium and aluminum during solidification. The sharp demarcation between the HAZ and the fusion zone is consistent with the extremely steep temperature gradient that occurs after laser melting.

Figure 7 presents the microhardness test results across the melt cross section. Microhardness is maximum at the surface and almost twice the hardness of the base material. As distance from the surface increases, microhardness reduces to base material hardness.

Figure 8 shows a corrosion diagram (anodic tests) for laser-treated and untreated samples. In general, the increase in current and the change in the electrode potentials of titanium and niobium decrease the dc resistance of Ti-Al-Nb. When the sample surface is laser treated, significant improvement in corrosion resistance results. It should be noted that an increase in corrosion rate for the untreated sample may be due to existing β-phase alloy (Ref 9). The anodic corrosion test results are given in Table 1.

5. Conclusions

Several conclusions can be derived from the present work:

- The high cooling rate results in fine columnar β grains that grow epitaxially from the base metal substrate in toward the center of the fusion zone.
- The temperature gradient within the melt is very high, giving rise to a narrow HAZ.
- Microhardness tests indicate that hardness at the workpiece surface increases to almost twice the base material hardness. As distance from the surface increases, hardness decreases.
- Corrosion tests show that corrosion resistance of the workpiece improves in the case of laser-treated samples. In general, niobium acts as a cathodic protector to titanium, reducing corrosion resistance.

References

1. W. Zang, G. Chen, Y. Wang, and Z. Sun, Characteristics of Heat Resistance Alloys Ti10Nb45Al and Ti18Nb48Al, *Scr. Metall.*, Vol 28 (No. 9), 1993, p 1113-1118
2. S.C. Jha, R. Ray, K.R. Teal, and F.H. Froes, Properties of Ti_3Al + Nb Alloys Produced via Rapid Solidification Technology, *Proc. 6th World Conf. Titanium*, 1988, p 961-966
3. A.I. Gardienko, Hardening Heat Treatment for Titanium Alloys, *Metalloved. Term. Obrob. Met.*, Vol 3, 1987, p 28-31
4. V.N. Moiseev, Prospects for the Development of a Hardening Heat Treatment for Titanium Alloys, *Metalloved. Term. Obrob. Met.*, Vol 10, 1977, p 63-68
5. A.I. Shcherbekov, V.N. Dorofervo, and N.O. Tomashov, Electrochemical and Corrosion Studies of Titanium-Niobium Alloys in Sulphuric Acid, Institute of Physical Chemistry, Academy of Sciences of the USSR, trans. from *Zashch. Met.*, Vol 26 (No. 5), 1990, p 753-758
6. B.S. Yilbas, Heating of Metals at a Free Surface by Laser Irradiation—An Electron Kinetic Theory Approach, *Int. J. Eng. Sci.*, Vol 24 (No. 8), 1985, p 1325-1334
7. F.W. Sears and G.L. Salinger, *Thermodynamics, Kinetic Theory, and Statistical Thermodynamics*, 3rd ed., Addison-Wesley, London, 1986
8. B.S. Yilbas, Optical Methods for Measurement of the Temporal Variation of Temperature at the Surface of a Metal Heated by a Laser Beam, *J. Opt.*, Vol 5 (No. 4), 1986, p 108-116
9. M.J. Park, A. Leyland, and A. Matthews, Corrosion Performance of Layered Coatings Produced by Physical Vapor Deposition, *Surf. Coat. Technol.*, Vol 43-44, 1990, p 481-492